APPLICATIONS OF
MODELLING AND SIMULATION
http://arqiipubl.com/ams eISSN 2600-8084 VOL 9, 2025, 374-388

Model Predictive Control for a Permanent Magnet Synchronous Motor Subject to Actuation Fault

Abdulkadir O. Nurudeen[1], Oyedotun E. Oyewole[2], Abdulrahman Babagana[2] and Isah A. Jimoh[2,*]

[1]Department of Mechanical Engineering, Glasgow Caledonian University, Glasgow, Scotland, UK
[2]Institute of Energy and Environment, Department of Electronic and Electrical Engineering, University of Strathclyde, Glasgow, UK

[*]Corresponding author: isah.jimoh@strath.ac.uk

Submitted 23 July 2025; Revised 06 September 2025; Accepted 02 October 2025; Available online 13 October 2025.

Abstract: Driven by the demand for greater energy efficiency and compact design, Permanent Magnet Synchronous Motors (PMSMs) have seen increasing adoption, gradually supplanting induction motors in applications like electric vehicles and household appliances. This paper investigates the constrained optimal control of the *d*-axis current and speed of a PMSM under the influence of external disturbances induced by load torque and scaling actuation faults in the *d*-*q* control voltages. To address this challenge, a fault-tolerant delta input form model predictive control (MPC) strategy is developed, which computes the input increment and compensates for the effects of uncertainty through the use of an observer that estimates the state and input vectors online. The proposed control scheme requires no modification to the standard MPC formulation based on the delta input form, except that the variables used to initialize the constrained optimal control problem are derived from the estimated state and input vectors. The performance of the control scheme is demonstrated through extensive simulations, which show its superiority over the conventional MPC strategy.

Keywords: Disturbance rejection; Fault-tolerant control; Model predictive control; Permanent magnet synchronous motor.

Notation	Description	Notation	Description
p	Number of pole pairs	i_d, i_q	Stator's *d*- and *q*-axis currents
J	Moment of inertia	V_d, V_q	Stator voltages in the same reference frame
R	Stator resistance	ω_r	Mechanical speed of the rotor
φ_m	Rotor flux	ω_e	Electrical speed of the rotor
L_d, L_q	Inductance in the *d*-*q* axis	T_e	Electromagnetic torque
B_v	Viscous coefficient	γ^i	Health indicators for *d*-axis voltage ($i = 1$) and *q*-axis voltage ($i = 2$) actuators
T_L	Load torque	p	Number of poles pair
x_p	State vector	u	Input vector
N	Prediction horizon	T_s	Sampling period
Q	Weighting matrices	P	Terminal weight matrix
u_{min}	Minimum limits on the *d*-*q* voltage input signals	u_{max}	Maximum limits on the *d*-*q* voltage input signals
$z(k)$	Controlled state without steady state offset	σ^i	Function of actuator health indicators with $i = 1, 2$

1. INTRODUCTION

Permanent Magnet Synchronous Motors (PMSMs) are rapidly gaining traction across both academic and industrial landscapes, outpacing traditional induction motors in high-performance applications. Their superior energy efficiency, compact structure, high torque-to-current ratio, and excellent dynamic response make them the preferred choice for next-generation systems in aerospace, marine propulsion, wind energy conversion, and heavy-duty machinery [1]-[3]. In response to increasing demands for compact design and improved energy efficiency, PMSMs have seen rising adoption, gradually displacing induction motors

in applications like electric vehicles and household appliances [4], [5]. Typically, PMSM drive systems employ a cascaded control architecture, consisting of inner-loop current regulators and an outer-loop speed controller, most commonly implemented using proportional-integral (PI) control schemes [6]. In this arrangement, the *d*- and *q*-axis currents are regulated independently, while the speed loop generates a reference for the *q*-axis current. However, due to physical constraints on motor currents and voltages, the system is susceptible to performance degradation during saturation, particularly in high-demand scenarios. To address these issues, anti-windup strategies [7], [8] have been developed to ensure stability and performance during constrained operation.

While PI-based control schemes are relatively simple and well-established, they are limited in their ability to handle multivariable interactions, system nonlinearities, and operational constraints directly. As such, there has been growing interest in advanced model-based control strategies that offer greater effectiveness and robustness under nonlinearities and external disturbances. Sliding Mode Control (SMC) has been extensively utilized for regulating the speed of PMSMs [9]. To enhance the capabilities of traditional SMC, particularly in terms of tracking accuracy, disturbance rejection, and chattering minimization, numerous improvement strategies have been introduced. These include modifications to the sliding surface, alternative reaching laws, higher-order SMC formulations, and hybrid approaches such as integration with artificial intelligence techniques or disturbance compensation schemes [10]-[13]. A comprehensive overview of these enhancement strategies for PMSM control using SMC can be found in [14].

In addition, several advanced control strategies have been proposed, such as backstepping control leveraging Lyapunov-based methods [15], active disturbance rejection control (ADRC) [16], and robust H_∞ control [17]. Model Predictive Control (MPC) has emerged as a promising candidate in this regard. Unlike the aforementioned feedback control methods, MPC employs an optimization-based framework that uses a predictive model of the system to determine a sequence of control actions by minimizing a cost function subject to system dynamics and constraints [18]. The predictive nature of MPC allows it to anticipate future disturbances and acts accordingly, offering superior performance in terms of tracking, constraint handling, and robustness. Several variants of MPC have been developed, such as Generalized Predictive Control (GPC), Dynamic Matrix Control (DMC), and state-space-based formulations. These have found widespread use in process industries, where slower dynamics make real-time optimization more tractable. Nonetheless, progress in solving constrained optimal control problems (COCPs), coupled with improvements in multicore processing and the deployment of field-programmable gate arrays (FPGAs), have significantly helped to alleviate these computational challenges [19].

In the context of PMSM control, MPC is particularly attractive for several reasons. First, the electrical dynamics of PMSMs can be modelled as multi-input, multi-output (MIMO) system in a rotating d–q reference frame, making them suitable for state-space MPC design. Second, these systems are often subject to constraints that MPC can naturally accommodate. Third, MPC can be extended to address persistent disturbances and repetitive tasks by incorporating disturbance observers or embedded integrators, ensuring zero steady-state error. One of the core applications of MPC in PMSM has been in predictive current control problem where it has been considered a widely successful strategy [20], [21].

In the context of speed control, the authors in [22] proposed the use of MPC for PMSM speed control for vehicle power applications. However, this work did not consider the effects of external disturbances which can result in tracking inaccuracies in the standard MPC scheme. In [23], the operating range that an MPC based on a linear model can cover was extended by formulating the PMSM as a linear time-varying (LTV) model. Thus, the developed LTV-MPC updates its internal linear model at each time step to accurately capture the PMSM's nonlinear behavior across different speed regions. An adaptive discrete linear plant model (ADLPM) adjusts to changing machine parameters and operating points based on measured stator currents, speed, and load torque. In the flux-weakening region, a performance control algorithm (PCA) ensures high dynamic performance [23]. However, this strategy does not include integral action that can ensure offset-free control under the influence of persistent disturbances.

In [24], a velocity form MPC scheme was developed for PMSM *d*-axis current and speed control without steady state offset introduced by external load torque. The velocity form MPC was modified in [25] by incorporating a feedforward mechanism to minimize the cross-coupling effects of the electromotive force between the *d*- and *q*-axis in the voltage equation. The performance of the controller was shown to outperform PI-based feedforward strategies. One limitation of the velocity form MPC approach is its dependence on direct access to state velocity measurements for feedback [26]. In scenarios where these velocities cannot be measured directly, it becomes necessary to either deploy a state velocity observer or approximate the velocity signals through numerical differentiation techniques combined with appropriate filtering.

Another approach to achieving offset-free tracking is the so-called partial velocity or delta input form MPC strategy [27]. To the best of the authors' knowledge, this method has not yet been explored in the context of PMSM control, possibly because the velocity form MPC is already a well-established technique for ensuring offset-free performance, particularly in scenarios where observers are not required [18]. Motivated by the limitations of the velocity form MPC, which requires state derivatives as feedback to achieve offset-free tracking under persistent disturbances, this paper proposes a delta input form MPC strategy to achieve offset-free speed tracking in the presence of load torque disturbances. Furthermore, previous studies [22]-[25] have generally assumed ideal actuation, neglecting the effects of actuation faults. In [28], it was shown that *d*–*q* control voltages applied to wind turbines can experience scaling faults, significantly degrading controller performance. To address this, the proposed method adaptively estimates the combined state and voltage input vectors, which are then used as feedback in the MPC framework. This enables active compensation for disturbances caused by load torque, voltage scaling faults, or both. The main benefits of this paper compared to previous studies on PMSM speed control are summarized as follows:

(a) A delta input form MPC strategy to achieve offset-free speed regulation while maintaining zero *d*-axis current for efficient PMSM operation. In addition to addressing load torque disturbances, the proposed scheme explicitly considers scaling faults in the *d*–*q* control voltages.

(b) In contrast to the delta input formulation of MPC presented in [18, 27], the proposed approach does not require prediction model augmentation, thereby avoiding any increase in the dimensionality of the optimal control problem. One key advantage of the proposed approach is its seamless integration into existing designs, requiring only a modification to the initialization procedure.
(c) Unlike velocity form MPC approaches [24] [25], which require state derivatives as feedback, the proposed method avoids this requirement. Since *d–q* currents and rotor speed are typically measured in practice, estimating the remaining variables is straightforward.
(d) The effectiveness of the proposed control strategy is validated through a series of simulated case studies conducted under varying disturbance conditions. Its performance is benchmarked against two conventional approaches: a delta input form MPC lacking offset-free capability, and a velocity form MPC that incorporates offset-free tracking.

The remainder of this paper is organised as follows: Section 2 presents the electrical model of the PMSM and defines the control problem. Section 3 details the actuator fault-tolerant MPC design, including the formulation of the quadratic program (QP) used for online implementation. Section 4 provides extensive simulation results, and Section 5 concludes the paper.

2. PRELIMINARIES

2.1 PMSM Electrical Model

The mathematical model of the PMSM in the d–q rotating reference frame is given as follows [29]:

$$\frac{di_d}{dt} = \frac{1}{L_d}\left(\gamma^1 V_d - Ri_d + \omega_e L_q i_q\right) \tag{1a}$$

$$\frac{di_q}{dt} = \frac{1}{L_q}\left(\gamma^2 V_q - Ri_q + \omega_e L_d i_d - \omega_e \varphi_m\right) \tag{1b}$$

$$\frac{d\omega_e}{dt} = \frac{p}{J}\left(T_e - \frac{B_v}{p} - T_L\right) \tag{1c}$$

$$T_e = \frac{3p}{2}\left\{\varphi_m i_q + \left(L_d - L_q\right) i_q i_d\right\} \tag{1d}$$

In which i_d and i_q are the stator's *d*- and *q*-axis currents, V_d and V_q are the stator voltages in the same reference frame and ω_e is the motor's electrical speed which is related to the mechanical speed of the rotor, ω_r, as $\omega_e = p\omega_r$ with p denoting the number of poles pairs. Also, B_v is the viscous coefficient and J is the total moment of inertia of the motor. Furthermore, T_L is the load torque which is unmeasured and thus is considered an unknown external asymptotically constant disturbance to be rejected by the controller. The variable R represents the stator's resistance and L_d and L_q denote the inductance of the stator in the *d-q* reference frame. The electromagnetic torque T_e is produced by two main phenomena – the reluctance torque generated by i_d and i_q and the permanent magnet generated flux, φ_m.

This work employs a surface-mounted PMSM, for which the electromagnetic torque T_e has a linear relationship with i_q, regardless of the value of the i_d current. Thus, it is given as follows:

$$T_e = \frac{3}{2} p \varphi_m i_q \tag{2}$$

In PMSM control, the *d*-axis current reference is typically set to zero during steady-state operation to improve energy efficiency (17). By maintaining $i_d = 0$, the electromagnetic torque T_e can be directly regulated through i_q, which is the fundamental principle of field-oriented control. Moreover, in the case of a surface-mounted PMSM, a type frequently used in real-world applications, the *d-q* axis inductances are equal, that is, $L_d = L_q$. In addition, γ^i with $i = 1{,}2$ denote the health indicators taking values in the interval (0,1] of the actuator voltages applied to the PMSM, where a value of '1' indicates fully functional actuation and '0' corresponds to total actuation failure [28]. This discussion focuses on partial loss cases, meaning that $\gamma^i > 0$.

2.2 Problem Formulation

The terms $\omega_e i_q$ and $\omega_e i_d$ in Equation (1a) and (1b), respectively, represent nonlinear cross-coupling components in the model. To facilitate the design of an MPC, these terms are typically linearized by approximating them around a specific operating point, thereby enabling the use of a linear model for prediction in the constrained optimal control problem so as to ensure that off-the-self solvers can be used to efficiently solve the resulting optimization problem.

The state vector and input vector are defined as follows:

$$\dot{x}_p = \begin{bmatrix} i_d \\ i_q \\ \omega_e \end{bmatrix} \in \mathbb{R}^n, \qquad u_p = \begin{bmatrix} V_d \\ V_q \end{bmatrix} \in \mathbb{R}^m$$

Then, the electrical model in Equation (1) can be written in a general form as follows:

$$\dot{x}_p = f(x_p, u_p, T_L, \gamma^i) \tag{3}$$

where $i = 1, 2$ and

$$f(x_p, u_p, T_L) = \begin{bmatrix} \frac{1}{L_d}(\gamma^1 V_d - Ri_d + \omega_e L_q i_q) \\ \frac{1}{L_q}(\gamma^2 V_q - Ri_q + \omega_e L_d i_d - \omega_e \varphi_m) \\ \frac{p}{J}\left(T_e - \frac{B_v}{p} - T_L\right) \end{bmatrix}$$

Since γ^i (i=1, 2) is unknown, the health statuses of the *d*-*q* voltages actuators can be defined as $\gamma^i = 1 - \sigma^i$ such that $0 \leq \sigma^i < 1$ which satisfies the condition that the system can only suffer from partial faults. With this definition, the nonlinear system in Equation (3) can be reformulated as follows:

$$\dot{x}_p = f(x_p, u_p) + d \tag{4}$$

$$f(x_p, u_p) = \begin{bmatrix} \frac{1}{L_d}(V_d - Ri_d + \omega_e L_q i_q) \\ \frac{1}{L_q}(V_q - Ri_q + \omega_e L_d i_d - \omega_e \varphi_m) \\ \frac{p}{J}\left(T_e - \frac{B_v}{p}\right) \end{bmatrix}, \qquad d = \begin{bmatrix} -\frac{\sigma^i}{L_d} V_d \\ -\frac{\sigma^i}{L_d} V_q \\ -\frac{p}{J} T_L \end{bmatrix}$$

Define the operating region for the PMSM around which the system is to be linearised as follows: i_{d0}, i_{q0} and ω_{e0}. The model can be linearized using the Jacobian approach to derive the linear state-space representation based on the chosen operating conditions. By neglecting the unknown disturbance terms due to both external load torque and scaling fault, the resulting linear state-space matrices are provided as:

$$\dot{x}_p = A_p x_p + B_p u \tag{5}$$

in which the system matrices are given as:

$$A_p = \begin{bmatrix} -\frac{R}{L_d} & \frac{L_q}{L_d}\omega_{e0} & \frac{L_q}{L_d} i_{q0} \\ \frac{L_d}{L_q}\omega_{e0} & -\frac{L_d}{L_q} & -\left(\frac{L_d}{L_q} i_{d0} - \frac{\varphi_m}{L_q}\right) \\ 0 & \frac{3}{2J} p^2 \varphi_m & -\frac{B_v}{J} \end{bmatrix}$$

$$B_p = \begin{bmatrix} \frac{1}{L_d} & 0 \\ 0 & \frac{1}{L_q} \\ 0 & 0 \end{bmatrix}$$

The continuous-time model in Equation (4) can be discretised using the zero-order-hold method to obtain the discrete-time model where the unmeasured disturbance d to obtain:

$$x_p(k+1) = A_d x_p(k) + B_d u(k) \tag{6}$$

Here, the matrices are given by:

$$A_d = e^{A_p T_s}, \quad B_d = \int_0^{T_s} e^{A_p \tau} B_p \, d\tau,$$

where T_s is the sampling period. Therefore, the control problem to be addressed in this paper is defined as follows. Given the discrete-time linear time-invariant state-space model (Equation (6)), the objective of this paper is to design a MPC scheme that ensures the PMSM speed, ω_e, accurately track an asymptotically constant reference electrical speed, ω_d^{ref}, while maintaining the *d*-axis current at $i_d^{ref} = 0$, thereby ensuring efficient operation of the PMSM despite the effects of load torque disturbances T_L, and *d*–*q* voltage scaling faults.

3. FAULT-TOLERANT CONTROL BASED ON DELTA INPUT FORM MPC

The design approach employed in this paper is aimed at implementing an MPC strategy which can deal with both disturbances and actuator faults without making significant modifications to the formulation of a conventional predictive controller where the delta input signal is considered in the objective function [18], [30].

3.1 MPC Design

This section presents the formulation of the predictive controller to be implemented in order to ensure robustness under load torque disturbance and actuation fault. To proceed, define the reference signal

$$x^{ref} = \begin{bmatrix} i_d^{ref} \\ i_q^{ref} \\ \omega_d^{ref} \end{bmatrix},$$

which the cost function to be minimized in each sampling instant is defined as follows:

$$J(x,u,N) = \frac{1}{2}\left\|x_p(k+j|k) - x^{ref}(k)\right\|_P + \frac{1}{2}\sum_{k=0}^{N-1}\left\|x_p(k+j|k) - x^{ref}(k)\right\|_Q + \|\Delta u(k+j|k)\|_R \tag{7}$$

where $x_p(k+j|k)$ denotes the j-th prediction of the state x_p sampling instant k, $\left\|x_p(k)\right\|_Q = x_p^T(k)Qx_p(k)$ and $\Delta u(k) = u(k) - u(k-1)$ is the delta input signal, representing the change in the input signal between two consecutive sampling period. Note that the goal is to primarily control the d-axis current i_q and the electrical speed ω_e to track a desired reference accurately which must be considered when implementing the control scheme. The weighting matrices for the state Q and the input R matrices to be defined as follows:

$$Q = \begin{bmatrix} q_1 & 0 & 0 \\ 0 & q_2 & 0 \\ 0 & 0 & q_3 \end{bmatrix} \text{ and } R = \begin{bmatrix} r_1 & 0 \\ 0 & r_2 \end{bmatrix},$$

Furthermore, P denotes the terminal weight matrix which is computed by solving the discrete-time algebraic Riccati equation

$$A_d{}^T P A_d - P + Q - A_d{}^T P B_d \left(R + B_d{}^T P B\right)^{-1} B_d^T P A_d = 0,$$

to enhance closed-loop stability under the constrained optimal control scheme. The delta input based cost function incorporates the previous control input, $u(k-1)$, as an extra state, thereby introducing integral action into the control loop. Based on the cost function (Equation (7)), the MPC problem is defined as follows:

$$\min_{\Delta u(k|k),\ldots,\Delta u(k+N-1|k)} J(x_p,u,N) \tag{8a}$$
$$x_p(k+1+j|k) = A_d x_p(k+j|k) + B_d u(k+j|k), j = 1,\ldots,N-1 \tag{8b}$$
$$u_{min} \le u(k+j-1|k) \le u_{max}, j = 1,\ldots,N \tag{8c}$$
$$u(k+j|k) = \Delta u(k+j|k) + u(k+j-1|k) \tag{8d}$$
$$u(k+j-1|k) = u(k-1) \tag{8e}$$
$$x_p(k|k) = x_p(k) \tag{8f}$$

The variables u_{min} and u_{max} denote the minimum and maximum limits on the d-q voltage input signals that can be applied to the PMSM. The MPC scheme in Equation (8) can have its performance deteriorate significantly under persistent disturbances and/or actuation faults. The work aims to design a predictive controller such that the QP in Equation (8) is not significantly changed while ensuring that it is fault-tolerant and able to eliminate steady state error under persistent system disturbance.

The input increment constraint in Equation (8d) can be re-written such that the desired input sequence $u(k+j-1|k), j = 1,\ldots,N$ becomes a function of the input increment sequence $\Delta u(k+j-1|k),\ j = 1,\ldots,N$ to be computed and the previous input $u(k-1)$ as:

$$\begin{aligned} u(k|k) &= \Delta u(k|k) + u(k-1|k) \\ u(k+1|k) &= \Delta u(k+1|k) + u(k|k) \Rightarrow \Delta u(k+1|k) + \Delta u(k|k) + u(k-1|k) \\ &\vdots \\ u(k+j-1|k) &= u(k-1|k) + \sum_{i=0}^{j-1} \Delta u(k+i|k) \end{aligned} \tag{9}$$

In order to achieve a fault-tolerant and disturbance rejection property in the predictive controller (Equation (8)), the approach used to initialize the problem is changed. Rather than using the measured states and the previous control signal, an estimator is designed to estimate the combined state and input signals which makes it possible to actively estimate uncertainties in the actuators so as to improve the correctness of the predicted states in the optimization problem. To estimate the state and input signal, the so-called *partial velocity model* [26] is formulated. This is based on the following equations:

$$\begin{aligned} x_p(k+1) &= A_d x_p(k) + B_d u(k) \\ u(k) &= \Delta u(k) + u(k-1) \end{aligned} \tag{10}$$

Thus, Equation (10) can be combined to obtain the extended state model:

$$\begin{bmatrix} x_p(k+1) \\ u(k) \end{bmatrix} = \begin{bmatrix} A_d & B_d \\ 0_{m\times n} & I_m \end{bmatrix} \underbrace{\begin{bmatrix} x_p(k) \\ u(k-1) \end{bmatrix}}_{\hat{x}(k)} + \begin{bmatrix} B_d \\ I_m \end{bmatrix} \Delta u(k) \tag{11a}$$

$$z(k) = M_p x_p(k) \tag{11b}$$

where $z(k)$ denotes the number of states to be controlled without steady state offset.

$$M_p = \begin{bmatrix} 1 & 0 & 0 \\ 0 & 0 & 1 \end{bmatrix}.$$

Notice that, for the purpose of estimator design, only the PMSM outputs $z(k)$ that need to be controlled without steady-state offset, caused by actuation faults and external disturbances, are considered as the outputs. This approach ensures that the observability of the extended model is preserved, as the number of outputs must be greater than or equal to the number of inputs to ensure accurate control [18]. Based on the extended model (Equation (11)), an observer of the following form can be implemented:

$$\begin{bmatrix} \hat{x}_p(k+1) \\ \hat{u}(k) \end{bmatrix} = \begin{bmatrix} A_d & B_d \\ 0_{m\times n} & I_m \end{bmatrix} \begin{bmatrix} \hat{x}_p(k) \\ \hat{u}(k-1) \end{bmatrix} + \begin{bmatrix} B_d \\ I_m \end{bmatrix} \Delta u(k) + L\big(z(k) - M_a \hat{x}(k)\big) \tag{12}$$

where $M_a = \begin{bmatrix} 1 & 0 & 0 & 0 & 0 \\ 0 & 0 & 1 & 0 & 0 \end{bmatrix}$ and $L \in \mathbb{R}^{(\boldsymbol{n+m})\times \boldsymbol{m}}$ is the observer gain to be computed and $\hat{x}_p(k)$ is the estimate of $x_p(k)$.

In this work, the observer gain is computed using Kalman filtering technique which requires the definition of the covariance weighting matrices $Q_w \in \mathbb{R}^{5\times 5}$ and $R_v \in \mathbb{R}^{2\times 2}$, respectively. Details on the implementation of a Kalman filter for state estimation can be found in [31]. Based on the estimated state and input signals in every time step, the MPC problem to be solved in each time step is formulated as follows:

$$\min_{\Delta u(k|k),\ldots,\Delta u(k+N-1|k)} J\big(x_p, u, N\big) \tag{13a}$$

$$x_p(k+1+j|k) = A_d x_p(k+j|k) + B_d u(k+j|k), j = 1, \ldots, N-1 \tag{13b}$$

$$u_{min} \le u(k+j-1|k) \le u_{max}, j = 1, \ldots, N \tag{13c}$$

$$u(k+j-1|k) = u(k-1|k) + \sum_{i=0}^{j-1} \Delta u(k+i|k) \tag{13d}$$

$$u(k+j-1|k) = \hat{u}(k-1) \tag{13e}$$

$$x_p(k|k) = \hat{x}_p(k) \tag{13f}$$

Therefore, the MPC to be solved is presented in Equation (13) to ensure the scheme is tolerant to fault and persistent disturbances. In the next subsection, the QP to be solved to implement the proposed constrained optimal control scheme is formulated.

3.2 Quadratic Program Formulation

A compact QP that can be solved by conventional QP solvers is presented. The discrete-time model in Equation (6) can be used for prediction over the user defined prediction horizon N. The state prediction is given as

$$\overbrace{\begin{bmatrix} x_p(k+1|k) \\ x_p(k+2|k) \\ \vdots \\ x_p(k+N|k) \end{bmatrix}}^{X} = \overbrace{\begin{bmatrix} A \\ A^2 \\ \vdots \\ A^N \end{bmatrix}}^{\Phi} x_p(k) + \overbrace{\begin{bmatrix} B & 0 & \cdots & 0 \\ AB & B & \cdots & 0 \\ \vdots & \vdots & \ddots & \vdots \\ A^{N-1}B & A^{N-2}B & \cdots & B \end{bmatrix}}^{\Psi} \overbrace{\begin{bmatrix} \Delta u(k|k) \\ \Delta u(k+1|k) \\ \vdots \\ \Delta u(k+N-1|k) \end{bmatrix}}^{\Delta U} \tag{14}$$

Similarly, the input signal in Equation (13d) can be written in the compact form:

$$\underbrace{\begin{bmatrix} u(k|k) \\ u(k+1|k) \\ \vdots \\ u(k+N-1|k) \end{bmatrix}}_{U} = \underbrace{\begin{bmatrix} I_m & 0 & \cdots & 0 \\ I_m & I_m & & 0 \\ \vdots & \vdots & \ddots & \vdots \\ I_m & I_m & \cdots & I_m \end{bmatrix}}_{G} \underbrace{\begin{bmatrix} \Delta u(k|k) \\ \Delta u(k+1|k) \\ \vdots \\ \Delta u(k+N-1|k) \end{bmatrix}}_{\Delta U} + \underbrace{\begin{bmatrix} I_m \\ I_m \\ \vdots \\ I_m \end{bmatrix}}_{\tilde{I}_m} u(k-1|k) \tag{15}$$

Based on Equation (14), the input inequality constraint in Equation (12c) can also be re-written in the compact form. Define the input limits over the prediction horizon, N, as

$$U_{max} = \begin{bmatrix} u_{max} \\ \vdots \\ u_{max} \end{bmatrix} \in \mathbb{R}^{Nm\times 1} \text{ and } U_{min} \begin{bmatrix} u_{min} \\ \vdots \\ u_{min} \end{bmatrix} \in \mathbb{R}^{\mathrm{Nm}\times 1}$$

Consequently, the input constraint over the horizon N can be written as

$$U_{min} \leq U \leq U_{max} \tag{16}$$

Substitute Equation (14) into Equation (15) to obtain:

$$U_{min} - \tilde{I}_m u(k-1|k) \leq G\Delta U \leq U_{max} - \tilde{I}_m u(k-1|k) \tag{17}$$

The inequality in Equation (17) can be re-written in the alternate form

$$\begin{aligned} -G\Delta U(k) &\leq -U_{min} + \tilde{I}_m u(k-1|k) \\ G\Delta U(k) &\leq U_{max} - \tilde{I}_m u(k-1|k) \end{aligned} \tag{18}$$

Based on Equation (18), the constraint to be implemented in the QP is given as

$$\underbrace{\begin{bmatrix} -G \\ G \end{bmatrix}}_{A_{in}} \Delta U \leq \underbrace{\begin{bmatrix} -U_{min} \\ U_{max} \end{bmatrix}}_{b_{in}} + \underbrace{\begin{bmatrix} \tilde{I}_m \\ -\tilde{I}_m \end{bmatrix}}_{B_{in}} u(k-1|k) \tag{19}$$

For brevity, notice that the cost function of the form in Equation (7) can be transformed into the following by neglecting the constant term that depends only on the reference state.

$$\begin{aligned} J(x_p, u, N) = {}^1\!/_2\, X(k)^T \underbrace{\begin{bmatrix} Q & \cdots & \cdots & 0 \\ \vdots & \ddots & \vdots & \vdots \\ \vdots & \cdots & Q & \vdots \\ 0 & \cdots & \cdots & P \end{bmatrix}}_{\mathcal{Q}} X(k) - (X^{ref})^T \underbrace{\begin{bmatrix} Q & \cdots & \cdots & 0 \\ \vdots & \ddots & \vdots & \vdots \\ \vdots & \cdots & Q & \vdots \\ 0 & \cdots & \cdots & P \end{bmatrix}}_{\mathcal{Q}} X(k) \\ + {}^1\!/_2\, \Delta U(k)^T \underbrace{\begin{bmatrix} R & \cdots & 0 \\ \vdots & \ddots & \vdots \\ 0 & \cdots & R \end{bmatrix}}_{\mathcal{R}} \Delta U(k) \end{aligned} \tag{20}$$

where $X^{ref} = \begin{bmatrix} x^{ref} \\ \vdots \\ x^{ref} \end{bmatrix} \in \mathbb{R}^{Nn\times 1}$

By substituting Equation (13) into Equation (20) and simplifying the resulting expression, and then expanding the resulting expression while eliminating the constant terms since they have no effect on the optimization problem solution, the resulting penalty function is given by,

$$J(x_p, u, N) = \frac{1}{2}\Delta U^T \mathcal{H} \Delta U + \hbar\left(x_p(k|k)\right)^T \Delta U \tag{21}$$

where $\mathcal{H} = (\Psi^T \mathcal{Q} \Psi + \mathcal{R})$ and $\hbar(x_p(k|k)) = \Psi^T \mathcal{Q}(\Phi x_p(k|k) - X^{ref} + \Psi \Delta U(k)$

Hence, the QP to be solved online is given by

$$\min_{\Delta u(k|k),\ldots,\Delta u(k+N-1|k)} J(x_p, u, N) = \frac{1}{2}\Delta U^T \mathcal{H} \Delta U + \hbar\left(x_p(k|k)\right)^T \Delta U \tag{22a}$$

$$A_{in}\Delta U \leq b_{in} + B_{in} u(k-1|k) \tag{22b}$$

$$u(k+j-1|k) = \hat{u}(k-1) \tag{22c}$$

$$x_p(k|k) = \hat{x}_p(k) \tag{22d}$$

In summary, QP in Equation (22) is solved using a quadratic solver to implement the fault-tolerant control strategy based on the delta input form of MPC as demonstrated in Figure 1.

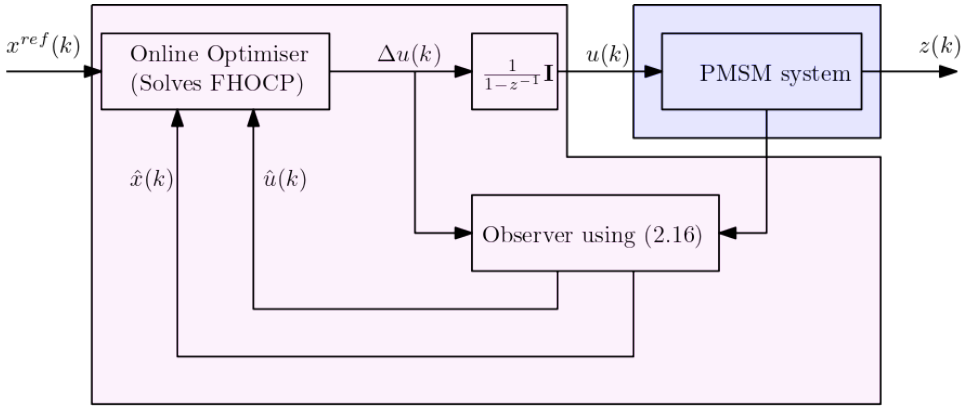

Figure 1. Block diagram representing the proposed fault-tolerant delta input form MPC strategy.

4. SIMULATED CASE STUDIES

To validate the developed fault-tolerant control strategy, the PMSM model [25] based on realistic and experimentally validated parameters presented in Table 1 are employed. The *d*-*q* axis control voltages are constrained as follows: $-25.17 \leq V_d \leq 25.17$, $-51.96 \leq V_q \leq 51.96$. To implement the controller, the prediction horizon is chosen as $N = 6$ and the weighting matrices are tuned as follows: $q_1 = 100, q_2 = 0.01, q_2 = 1$ and $r_1 = r_2 = 1$. Notice that the *q*-axis current receives the least weight because there is no requirement for this state to track a specific reference without steady-state error. The terminal gain weight P is obtained by solving the discrete-time Riccati equation. The Kalman filter is implemented by choosing $Q_w \in \mathbb{R}^{5\times5}$ and $R_v \in \mathbb{R}^{2\times2}$ as identity matrices. The sampling time used to implement the discrete control is given as T_s =2 ms. In this study, the PMSM is required to track varying speed reference

$$\omega_d^{ref} = \begin{cases} 200\ rpm, & \text{for } t \leq 0.45\ s \\ 300\ rpm, & \text{for } 0.45\ s \leq t \leq 1\ s \\ 250\ rpm, & \text{for } t \geq 1\ s \end{cases} \tag{23}$$

while ensuring the $i_d^{ref} = 0$ A to ensure efficient operation of the PMSM. Note that i_q^{ref} is arbitrarily set to zero but there is no requirement to maintain this value. Furthermore, the effects of measurement noise are considered, since in practice, it is not possible to obtain perfect measurements. In this work, additive white Gaussian measurement noise with a signal-to-noise ratio of 30 dB is assumed to affect all state measurements. The performance of the controllers is evaluated using quantitative performance metrics based on the RMS tracking error (RMSE) for the *d*-axis current and the motor speed computed as follows:

$$MSE = \sqrt{\frac{1}{T_f}\sum_{k=1}^{T_f}\left(x_p(l,k) - x^{ref}(l,k)\right)^2}\ , l = 1 \text{ or } 3 \tag{24}$$

where T_f represents the simulation duration and $l = 1, 3$, denotes the *d*-axis current and motor speed, respectively, in (24). In addition, the input chattering is computed based on the RMS value of the input increment between consecutive time steps as follows:

$$Input\ Chattering = \sqrt{\frac{1}{T_f}\sum_{k=1}^{T_f}(\Delta u(l,k))^2}, \qquad l = 1 \text{ or } 2 \tag{25}$$

In Equation (25), $l = 1, 2$ reprsent the *d*-axis and *q*-axis control voltages. The performance of the proposed controller, denoted MPC1, is evaluated across three case studies to demonstrate its effectiveness compared to the standard MPC variant described in Equation (8), denoted MPC2, as well as the velocity form MPC [24] [29], denoted MPC3. The results are presented in the following subsections.

Table 1. PMSM parameters.

Notation	Description	Value	Unit
p	Number of pole pairs	2	-
J	Moment of inertia	2.35×10^{-4}	Kg.m^2
R	Stator resistance	2.98	Ohm
φ_m	Rotor flux	0.125	Wb
L_d, L_q	Inductance in the *d*-*q* axis	7×10^{-3}	H
B_v	Viscous coefficient	1.1×10^{-4}	-

4.1 Scenario 1: Performance Under Step Change In Load Torque Without Actuator Faults

In this scenario 1, the PMSM is simulated under the assumption that the *d-q* control voltages are correctly applied to the PMSM with no form of scaling error. As a consequence, $\sigma^i = 0$ for $i = 1,2$. However, during the operation of the system at time 1 seconds, the system transitions from no external load torque condition to a non-zero torque as described below.

$$T_L = \begin{cases} 0\ Nm, & for\ t \leq 1.0\ s \\ 1\ Nm, & for\ t \geq 1.0\ s \end{cases} \tag{26}$$

The primary objective of the control system is to achieve accurate and robust speed tracking despite the influence of unmeasured and abrupt changes in external load torque. Simultaneously, the controller must ensure that the *d*-axis current is maintained at zero to promote energy-efficient operation of the PMSM. As illustrated in Figure 2, the proposed fault-tolerant MPC1 strategy demonstrates a strong disturbance rejection capability. When subjected to a sudden change in load torque, the controller swiftly corrects the deviation and restores the system to its desired steady-state performance. This behavior validates the scheme's ability to preserve closed-loop stability and track the reference speed asymptotically, even in the presence of plant-model mismatch induced by unknown disturbances. The input voltages of MPC1 and MPC3 are adjusted to counteract the load torque disturbance, as illustrated in Figure 3.

In contrast, the conventional MPC2 strategy, formulated in the $\Delta u(k)$ −form and lacking an active state and input estimation mechanism, exhibits significant steady-state errors. Notably, the speed tracking error exceeds up to 80 rpm, while the *d*-axis current deviates by approximately 0.35 A, indicating poor disturbance rejection and a lack of integral-like behaviour in the controller structure. The velocity form MPC3 successfully achieved offset-free tracking in this scenario, demonstrating faster convergence and less overshoots compared to the proposed MPC1. Nevertheless, the results highlight the effectiveness of the fault-tolerant MPC1 scheme in maintaining accurate steady-state speed regulation, comparable to MPC3, while also suppressing undesired current components under uncertain conditions.

Figure 4 illustrates the estimated *d*–*q* voltages, $\hat{V}_d$ and $\hat{V}_q$ obtained using a Kalman filtering approach, which are employed in the predictive mechanism of the fault-tolerant MPC1 control strategy. These estimated signals are displayed alongside the corresponding actual voltage inputs applied to the PMSM. As observed in the figure, the Kalman-based estimation makes it possible to compensate for the effect of disturbances via the introduced estimation error that is dependent on the error induced by the external load torque. By driving the PMSM to mitigate the load torque induced error, the controller is able to reliably track the desired reference trajectories and fulfill the control objectives.

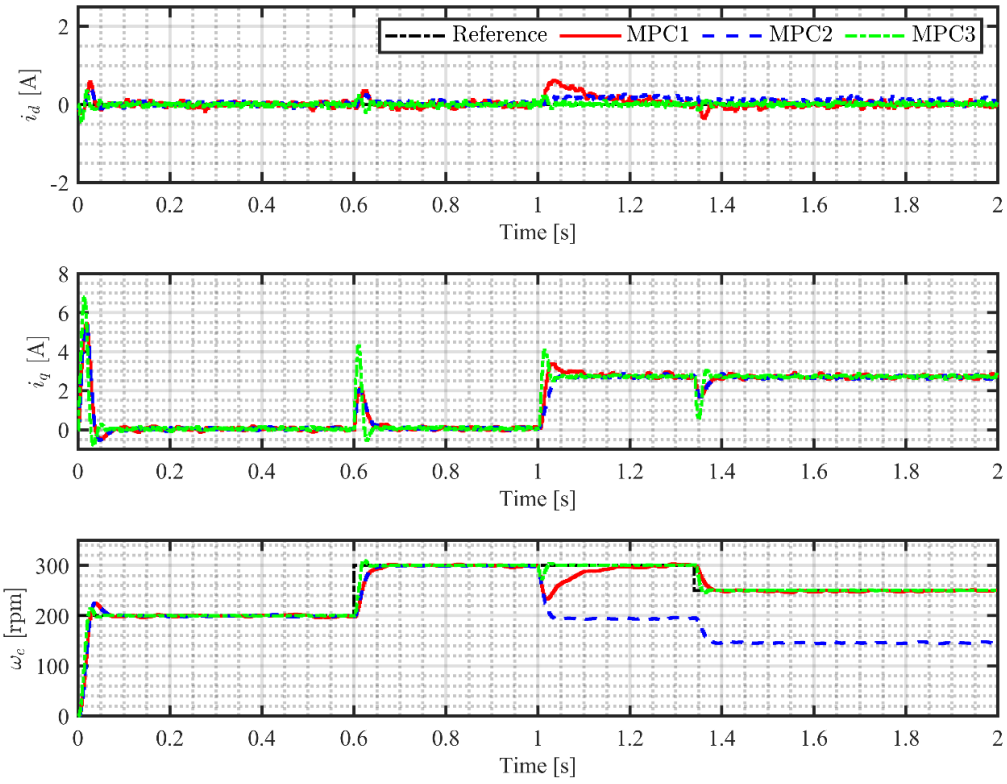

Figure 2. Scenario 1: Closed-loop evolution of the PMSM states variables based on MPC1, MPC2 and MPC3 strategies.

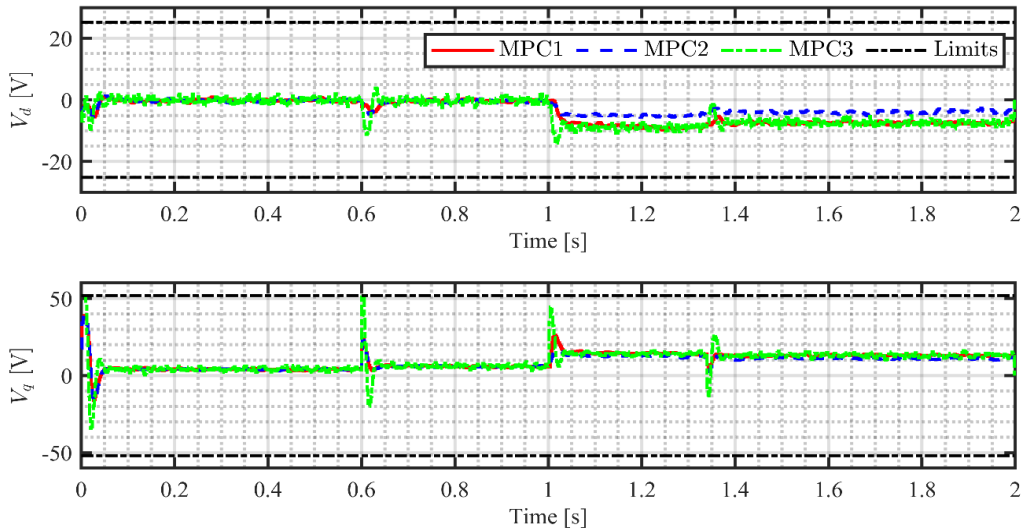

Figure 3. Scenario 1: Control *d-q* voltages evolution under MPC1, MPC2 and MPC3 strategies.

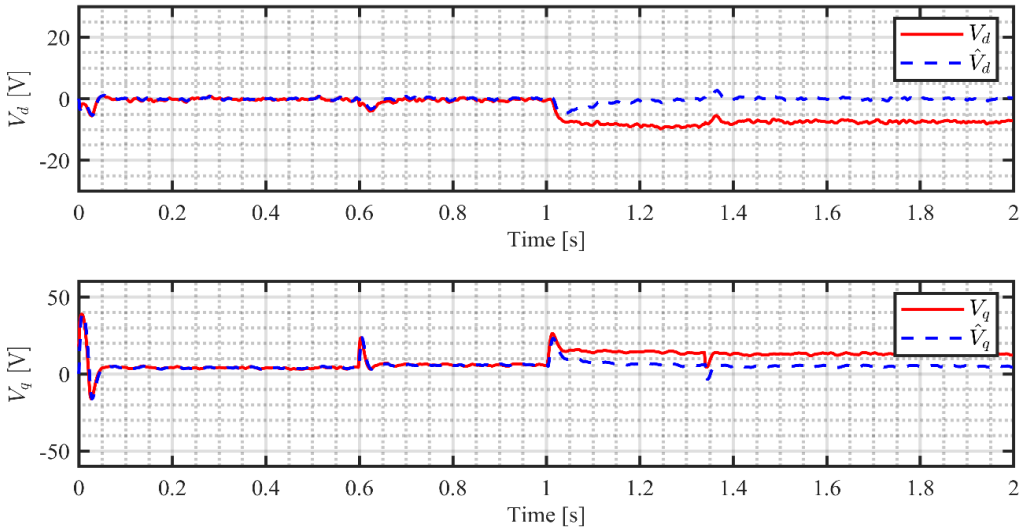

Figure 4. Scenario 1: The actual and estimated control *d-q* voltages under the fault-tolerant delta input form MPC1.

4.2 Scenario 2: Performance Under No Load Conditions with Actuator Scaling Faults

This section presents an evaluation of the proposed control scheme under no-load operating conditions, specifically in the presence of scaling faults in the *d-q* voltages. The goal is to investigate the controller's ability to maintain desired performance despite the introduction of fault conditions that can significantly affect the system's actuation capability. Under no-load conditions $T_L = 0$ Nm for all t, the system operates without any mechanical load applied to the shaft, thus isolating the influence of external torque disturbances and allowing a focused assessment of fault-related dynamics. This scenario is simulated by considering $\sigma^1 = \sigma^2$, where both signals are generated as follows:

$$\sigma^i = \begin{cases} 0, & \text{for } t \leq 1.0\ s \\ 0.6, & \text{for } t \geq 1.0\ s \end{cases} \tag{27}$$

The results obtained are presented in Figures 5-7. Figure 5 displays the state variables, where it can be observed that upon the introduction of the actuation scaling fault, the proposed MPC1 controller successfully mitigates the tracking error induced by the fault. In contrast, the conventional MPC2 scheme exhibits persistent tracking deviations, primarily due to inaccuracies in scaling the *d–q* control voltages. Specifically, the fault introduces a speed tracking error of approximately 38 rpm when the reference speed is set to 300 rpm, and about 18 rpm for a reference speed of 250 rpm. Under the actuator fault conditions, MPC3 exhibits pronounced oscillatory behaviour, particularly in the input signals. This scenario effectively highlights the robustness of the proposed control scheme, which maintains stable performance and mitigates fault-induced disturbances more effectively. Analogous to the disturbance caused by the load torque in Scenario 1, the estimated input signals are adaptively adjusted relative to the actual input signals applied to the PMSM. This modification enables the fault-tolerant strategy to compensate for the expected tracking errors that would otherwise arise in the *d*-axis current and the electrical speed response of the motor compensate for the expected tracking errors that would otherwise arise in the *d*-axis current and the electrical speed response of the motor speed response of the motor of the motor compensate for the expected tracking errors that would otherwise arise in the *d*-axis current and the electrical speed response of the motor.

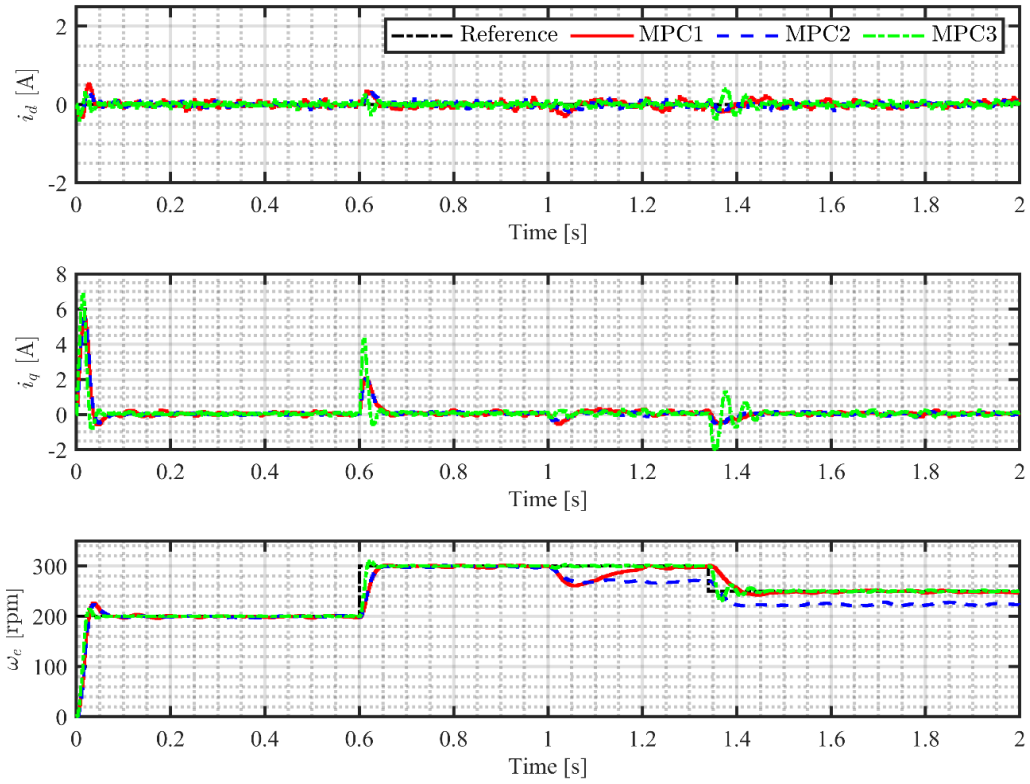

Figure 5. Scenario 2: Closed-loop evolution of the PMSM drive states under the MPC1, MPC2 and MPC3 strategies.

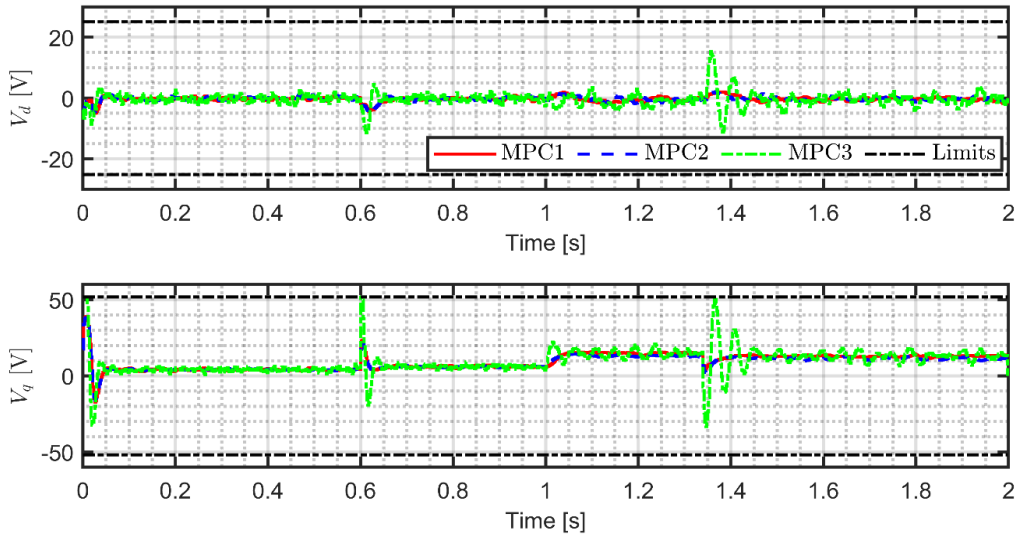

Figure 6. Scenario 2: Control *d*-*q* voltages evolution for MPC1, MPC2 and MPC3 strategies.

4.1 Scenario 3: Performance Under Step Change in Load Torque with Actuator Scaling Faults

The performance of the proposed control strategy is examined under the influence of a combined disturbance scenario, which includes both load torque variation and inaccuracies introduced by scaling the *d*–*q* control voltages. As illustrated in Figure 8, the standard MPC2 framework exhibits substantial tracking errors, particularly evident in the *d*-axis current and the electrical speed response of the PMSM. Although the proposed fault-tolerant MPC1 controller requires a comparatively longer settling time relative to the earlier two test scenarios, it ultimately succeeds in accurately tracking the reference *d*-axis current and electrical speed. Due to the challenging nature of Scenario 3, which involves both load torque disturbance and actuator fault, MPC3 encounters infeasibility during execution. Consequently, its results are omitted from the figures associated with this scenario. The results further reinforce the superiority of the proposed MPC1 scheme when subjected to complex additive disturbances, including load torque variations and actuator fault-induced uncertainties. Unlike the alternative strategy (that is, velocity form MPC) that exhibits instability or infeasibility under such conditions with constraints, MPC1 consistently maintains accurate speed regulation and effectively suppresses undesired current components. Its fault-tolerant design ensures reliable performance even in scenarios where conventional MPC formulations, such as MPC3, fail to converge or suffer from oscillatory behavior.

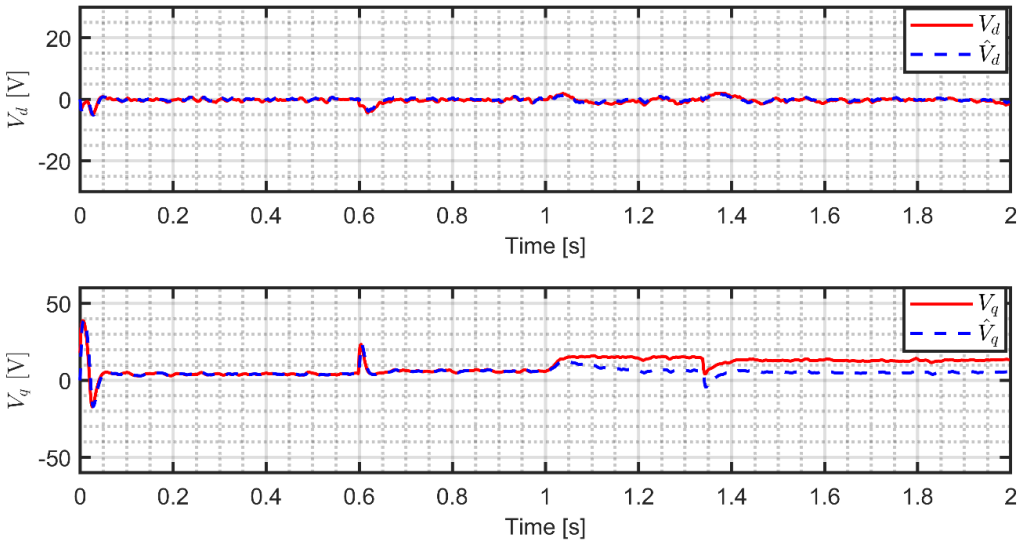

Figure 7. Scenario 2: Control *d-q* voltages evolution under MPC1 and MPC2 strategies.

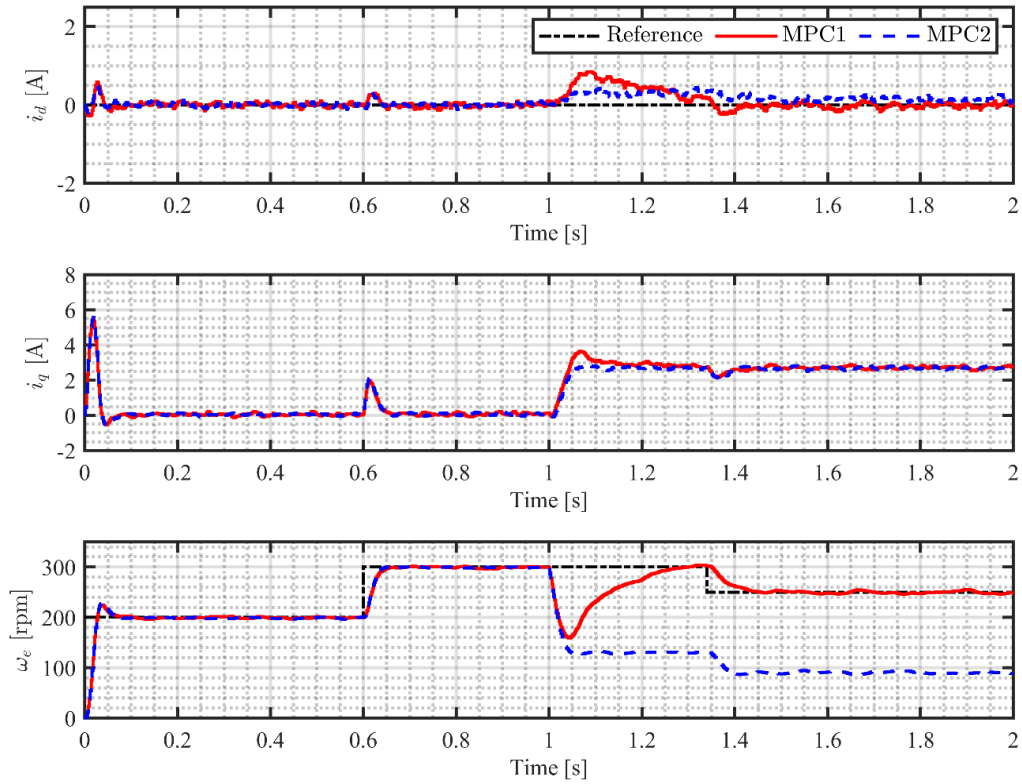

Figure 8. Scenario 3: Closed-loop response of the PMSM drive states under MPC1 and MPC2 strategies. MPC3 becomes infeasible in this case study.

Figure 9 presents the input *d–q* voltage signals applied to drive the PMSM, demonstrating the adaptiveness of the proposed scheme as the applied input is significantly modified to account for the effects of the uncertainties. Furthermore, the comparison shown in Figure 10 reveals a noticeable deviation between the estimated and the actual applied voltages, demonstrating the discrepancy addressed by the MPC1 scheme. The enhanced control performance is primarily attributed to the observer-based compensation mechanism embedded within the MPC1 framework, which effectively accounts for unmeasured disturbances. This compensation ensures a close alignment between the predicted system behavior and the actual dynamic response, thereby reinforcing the robustness of the proposed control approach.

Furthermore, the performance of the controllers evaluated in this simulation study is summarized using RMSE and input chattering metrics, as presented in Table 2. Notably, MPC3 demonstrates superior tracking accuracy in terms of RMSE compared to both MPC1 and MPC2. However, the proposed MPC1 exhibits significantly better performance in suppressing input chattering induced by load torque disturbances and measurement noise. Moreover, MPC1 was the only controller capable of successfully rejecting disturbances in Scenario 3, where MPC3 failed due to infeasibility under the input constraints.

Table 2. Controllers' performance comparison based on RMS values of errors and input chattering.

Scenario	Controller	RMSE		Input Chattering	
		i_d	ω_e	V_d	V_q
1	MPC1	0.13	2.15	0.20	0.69
	MPC2	0.12	11.87	0.25	0.61
	MPC3	0.05	1.36	0.90	2.73
2	MPC1	0.074	2.00	0.17	0.59
	MPC2	0.057	3.36	0.23	0.60
	MPC3	0.065	1.20	0.95	2.71
3	MPC1	0.22	4.48	0.20	0.69
	MPC2	0.17	18.35	0.23	0.62
	MPC3	Not Feasible	Not Feasible	Not Feasible	Not Feasible

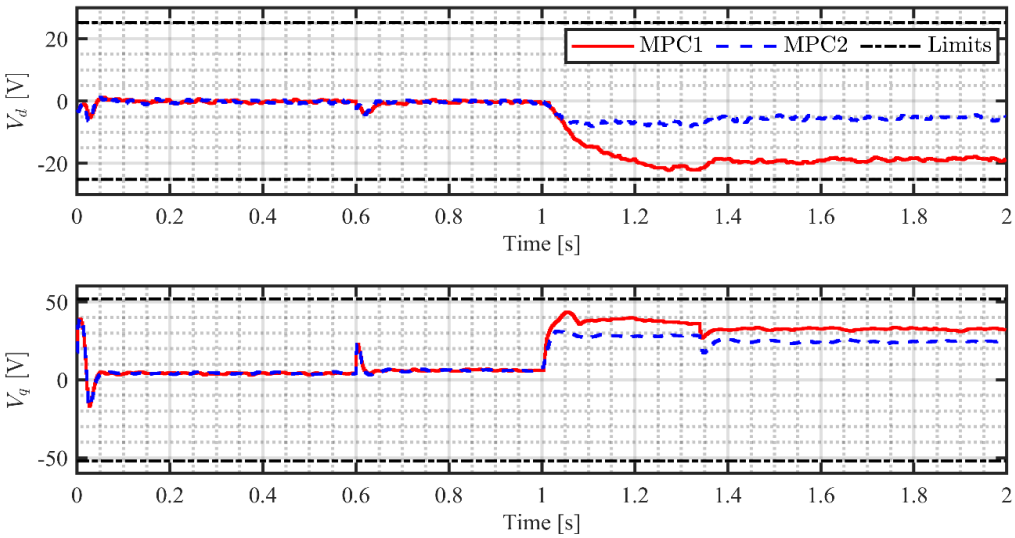

Figure 9. Scenario 3: Control *d-q* voltage evolution under the MPC1and MPC2 strategies. MPC3 becomes infeasibility in this case study.

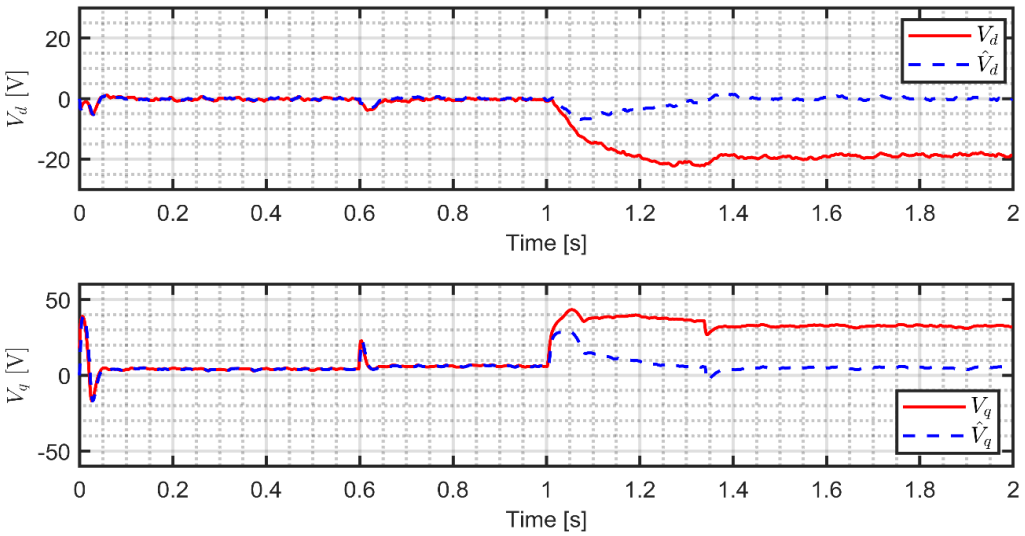

Figure 10. Scenario 3: The actual and estimated control *d-q* voltages under the fault-tolerant delta input form MPC1.

5. CONCLUSIONS

This study has presented a fault-tolerant control framework for Permanent Magnet Synchronous Motors (PMSMs), focused on the constrained optimal regulation of the *d*-axis current and rotational speed tracking control under the impact of external disturbances. By leveraging a delta input form MPC strategy enhanced with online state and input estimation, the proposed scheme effectively mitigates the influence of load torque variations and actuation scaling faults without altering the underlying MPC formulation. The only structural adjustment involves initializing the optimization problem using observer-derived

estimates, enabling robust and accurate predictive behavior in faulty operating conditions and in the presence of external disturbances. Through extensive simulation analysis, the developed control approach demonstrates superior performance when compared to conventional delta input form MPC method, confirming its effectiveness and resilience in disturbed operational conditions. These findings reinforce the viability of observer-integrated MPC strategies for enhancing control reliability in high-performance motor applications.

ACKNOWLEDGEMENT AND FUNDING

The authors receive no financial support for the research, authorship, and publication of this article.

DECLARATION OF CONFLICTING INTERESTS

The authors declare no potential conflicts of interest with respect to the research and publication of this article.

REFERENCES

[1] X. Sun, N. Xu, M. Yao, F. Cai and M. Wu, Efficient feedback linearization control for an IPMSM of EVs based on improved firefly algorithm, *ISA Transactions*, 134, 2023, 431-441.

[2] S. Niu, Y. Luo, W. Fu and X. Zhang, An indirect reference vector-based model predictive control for a three-phase PMSM motor, *IEEE Access*, 8, 2020, 29435-29445.

[3] A. Rassõlkin, A. Kallaste, S. Orlova, L. Gevorkov, T. Vaimann and A. Belahcen, Re-use and recycling of different electrical machines, *Latvian Journal of Physics and Technical Sciences*, 55(4), 2018, 13-23.

[4] J. Linares-Flores, C. Garcia-Rodriguez, H. Sira-Ramirez and O. D. Ramirez-Cardenas, Robust backstepping tracking controller for low speed PMSM positioning system: Design, analysis, and implementation, *IEEE Transactions on Industrial Informatics*, 11(5), 2015, 1130-1141.

[5] T. D. Do, H. H. Choi and J. -W. Jung, θ-D approximation technique for nonlinear optimal speed control design of surface-mounted PMSM drives, *IEEE/ASME Transactions on Mechatronics*, 20(4), 2015, 1822-1831.

[6] H. B. Shin, New anti-windup PI controller for variable-speed motor drives, *IEEE Transactions on Industrial Electronics*, 45(3), 1998, 445-450.

[7] M. Kerr, M. C. Turner, E. Villota, S. Jayasuriya and I. Postlethwaite, A robust anti-windup design procedure for SISO systems, *International Journal of Control*, 84(2), 2011, 351-369.

[8] Y. Peng, D. Vrancic and R. Hanus, Anti-windup, bumpless, and conditioned transfer techniques for PID controllers, *IEEE Control Systems Magazine*, 16(4), 1996, 48-57.

[9] F. M. Zaihidee, S. Mekhilef and M. Mubin, Application of fractional order sliding mode control for speed control of permanent magnet synchronous motor, *IEEE Access*, 7, 2019, 101765-101774.

[10] S. Li, M. Zhou and X. Yu, Design and implementation of terminal sliding mode control method for PMSM speed regulation system, *IEEE Transactions on Industrial Informatics*, 9(4), 2013, 1879-1891.

[11] S. Li, K. Zong and H. Liu, A composite speed controller based on a second-order model of permanent magnet synchronous motor system, *Transactions of the Institute of Measurement and Control*, 33(5), 2011, 522-541.

[12] H. Liu and S. Li, Speed control for PMSM servo system using predictive functional control and extended state observer, *IEEE Transactions on Industrial Informatics*, 59(2), 2012, 1171-1183.

[13] F. F. M. El-Sousy, Robust wavelet-neural-network sliding-mode control system for permanent magnet synchronous motor drive, *IET Electric Power Applications*, 5(1), 2011, 113-132.

[14] F. M. Zaihidee, S. Mekhilef and M. Mubin, Robust speed control of PMSM using sliding mode control (SMC) - A review, *Energies*, 12(9), 2019, 1669.

[15] J. Zhou and Y. Wang, Adaptive backstepping speed controller design for a permanent magnet synchronous motor, *IEE Proceedings: Electric Power Applications*, 149(2), 2002, 165-172.

[16] Y. X. Su, C. H. Zheng and B. Y. Duan, Automatic disturbances rejection controller for precise motion control of permanent-magnet synchronous motors, *IEEE Transactions on Industrial Electronics*, 52(3), 2005, 814-823.

[17] T. -L. Hsien, Y. -Y. Sun and M. -C. Tsai, H_∞ control for a sensorless permanent-magnet synchronous drive, *IEE Proceedings: Electric Power Applications*, 144(3), 1997, 173-181.

[18] A. Jimoh, I. B. Küçükdemiral, G. Bevan, and P. E. Orukpe, Offset-free model predictive control: A study of different formulations with further results, *Proceedings of the 2020 28th Mediterranean Conference on Control and Automation (MED)*, Saint-Raphaël, France, 2020, 671-676.

[19] H. Deng and T. Ohtsuka, A parallel newton-type method for nonlinear model predictive control, *Automatica*, 109, 2019, 108560.

[20] A. Brosch, O. Wallscheid, and J. Böcker, Model predictive control of permanent magnet synchronous motors in the overmodulation region including six-step operation, *IEEE Open Journal of Industry Applications*, 2, 2021, 47-63.

[21] M. Peña, M. Meyer, O. Wallscheid and J. Böcker, Model predictive direct self-control for six-step operation of permanent-magnet synchronous machines, *IEEE Transactions on Power Electronics*, 38(10), 2023, 12416-12429.

[22] A. A. Ahmed, Fast-speed drives for permanent magnet synchronous motor based on model predictive control, *Proceedings of the 2015 IEEE Vehicle Power and Propulsion Conference (VPPC)*, Montreal, Canada, 2015, 1-6.

[23] M. M. Ismail, W. Xu, J. Ge, Y. Tang, A. K. Junejo and M. G. Hussien, Adaptive linear predictive model of an improved

predictive control of permanent magnet synchronous motor over different speed regions, *IEEE Transactions on Power Electronics*, 37(12), 2022, 15338-15355.

[24] S. Chai, L. Wang and E. Rogers, Model predictive control of a permanent magnet synchronous motor with experimental validation, Control Engineering Practice, 21(11), 2013, 1584-1593.

[25] Y. Zhu, G. Xu, J. Yin and Y. Liu, Speed control of permanent magnet synchronous motor drives based on model predictive control, *Proceedings of the 2017 International Conference on Computer Technology, Electronics and Communication (ICCTEC)*, Dalian, China, 2017, 908-913.

[26] P. S. Cisneros and H. Werner, A velocity algorithm for nonlinear model predictive control, *IEEE Transactions on Control Systems Technology*, 29(3), 2020, 1310-1315.

[27] A. H. Gonzalez, E. J. Adam, and J. L. Marchetti, Conditions for offset elimination in state space receding horizon controllers: A tutorial analysis, Chemical Engineering and Processing: Process Intensification, vol. 47, no. 12, pp. 2184-2194, 2008.

[28] A. Jimoh, T. Zaman, M. Syed, H. Yue, G. Burt and M. S. El Moursi, Tube-based linear parameter-varying model predictive control for wind energy conversion systems, *IEEE Transactions on Sustainable Energy*, 16(2), 2024, 1225-1237.

[29] P. Pillay and R. Krishnan, Modeling of permanent magnet motor drives, *IEEE Transactions on Industrial Electronics*, 35(4), 1988, 537-541.

[30] G. Pannocchia, Offset-free tracking MPC: A tutorial review and comparison of different formulations, *Proceedings of the 2015 European Control Conference (ECC)*, Linz, Austria, 2015, 527-532.

[31] L. Wang, *Model predictive control system design and implementation using MATLAB*. Springer Science & Business Media, 2009.